Numerical Investigation on mixture formation and combustion process of innovative piston bowl geometries in a swirl-supported light-duty diesel engine

SAE INTERNATIONAL

ARTICLE INFO
Article ID: 03-14-02-0015

doi:10.4271/03-14-02-0015

Numerical Investigation on Mixture Formation and Combustion Process of Innovative Piston Bowl Geometries in a Swirl-Supported Light-Duty Diesel Engine

Federico Millo,[1] Andrea Piano,[1] Salvatore Roggio,[1] Andrea Bianco,[2] and Francesco Concetto Pesce[3]

[1]Politecnico di Torino, Italy
[2]Powertech Engineering, Italy
[3]PUNCH Torino S.p.A/ formerly General Motors Global Propulsion Systems, Italy

Abstract

In recent years, several innovative diesel combustion systems were developed and optimized in order to enhance the air and injected fuel mixing for engine efficiency improvements and to mitigate the formation of fuel-rich regions for soot emissions reduction. With these aims, a three-dimensional computational fluid dynamics (3D-CFD) numerical study was carried out in order to evaluate the impact of three different piston bowl geometries on a passenger car four-cylinder diesel engine, 1.6 liters. Once the numerical model was validated considering the baseline re-entrant bowl, two innovative bowl geometries were defined: one based on the stepped-lip bowl; the other including a number of radial bumps equal to the nozzle holes number. Firstly, the rated power engine operating condition was investigated under nonreacting conditions to evaluate the piston bowl effects on the in-cylinder mixing. Results highlight for both the innovative piston bowls better air utilization with respect to the re-entrant bowl: the stepped-lip bowl creates a dual toroidal vortex leading to a higher air/fuel mixing, while the radial-bumps bowl significantly affects the jet-to-jet interaction and promotes the recirculation of the fuel jet downstream to the bump, where the available oxygen enhances the mixing rate. After that, the combustion analysis was carried out for both rated power and partial-load engine operating conditions. Results confirmed that thanks to the better air-fuel mixing, the combustion process can be improved thanks to the innovative bowl designs, both increasing the engine efficiency at full-load condition and minimizing the engine-out soot emissions at partial-load operating point.

History

Received: 23 Jul 2020
Revised: 20 Sep 2020
Accepted: 17 Nov 2020
e-Available: 28 Dec 2020

Keywords

Diesel engine, Piston geometry, Numerical simulation, Spray-wall interaction

Citation

Millo, F., Piano, A., Roggio, S., Bianco, A. et al., "Numerical Investigation on Mixture Formation and Combustion Process of Innovative Piston Bowl Geometries in a Swirl-Supported Light-Duty Diesel Engine," *SAE Int. J. Engines* 14(2):2021, doi:10.4271/03-14-02-0015.

ISSN: 1946-3936
e-ISSN: 1946-3944

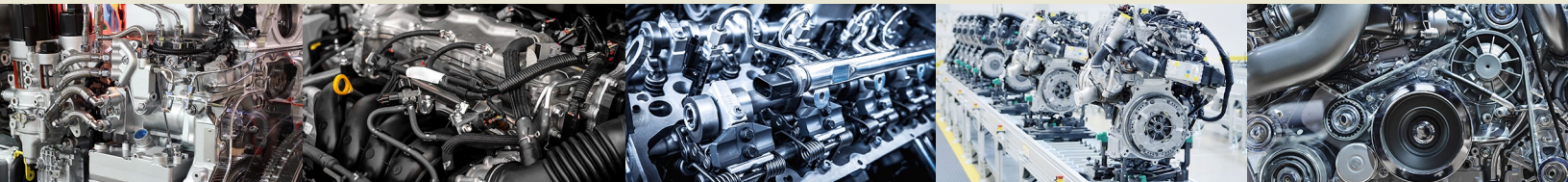

1. Introduction

In recent years, the need to comply with increasingly demanding carbon dioxide (CO_2) legislative targets, and the more stringent emission standards are requiring a considerable increment in diesel engines cost, noticeably affecting the market penetration in the next years [1]. In this context, the aftertreatment systems play a major role [2]; thus, to keep the engine cost down, the focus can move on the in-cylinder control of pollutant emissions by directly acting on the combustion process. It is well known that combustion chamber design is extremely effective in reducing both the fuel consumption and the engine-out pollutant emissions, mainly represented by oxides of nitrogen (NOx) and soot [3]; in fact, changing the spray-to-wall interaction can mitigate the formation of rich zones within the combustion chamber, enhancing the air utilization. Nevertheless, the combustion system optimization requires a deep understanding of the fuel jet interaction with the in-cylinder swirling flow and the piston bowl, as outlined by Miles and Andersson in [4].

In the last years, one of the main alternatives to the conventional re-entrant bowl was represented by the stepped-lip combustion systems [5, 6, 7, 8, 9]. The basic idea of such designs is to direct the injected fuel toward a chamfered lip creating two counter-rotating toroidal vortices inward into the bowl and outward onto the squish region, enhancing the air/fuel mixing and limiting the fuel propagation toward the cylinder liner [5]. Thanks to the enhanced mixing, a stepped-lip combustion system could adopt high Exhaust Gas Recirculation (EGR) rate for NOx control, maintaining a low soot-formation level, also thanks to higher injection pressure [10]. Moreover, to achieve an optimal fuel jet splitting at the bowl lip, a recalibration of the injection timing is required, as highlighted in [11]. In fact, as shown by Busch et al. [12], at partial-load engine operating conditions, a faster heat release rate (HRR) in the late combustion phase (50-90% of the burned mass fraction) can be observed only for a limited range of injection timing. These late-stage combusting flow structures, investigated through the combustion image velocimetry (CIV) technique by Zha et al. in [13], highlight a strong correlation between the enhanced burn rate and the formation of long-lasting toroidal vortices due to the stepped lip. In addition, even higher thermal efficiency could be reached with the stepped-lip bowl due to the reduced heat transfer losses, not only for the lower bowl surface area but also for the reduced flame penetration toward the cylinder liner, as Styron et al. suggested in [6]. As far as soot emission is concerned, the stepped-lip bowls showed soot attenuation, thanks to the more evenly distributed air/fuel mixing, which increases the oxidation rate in the late combustion phase [7]. This latter was confirmed by the natural luminosity (NL) analysis, performed in the framework of collaboration of the Engine Combustion Network (ECN) and available in [14], showing a longer soot residence time in the re-entrant bowl since the large toroidal vortex for the re-entrant bowl leads to an overall slower mixing, as also numerically investigated by Perini et al. in [15].

Among the combustion systems designed for low-swirl heavy-duty applications, the open bowl shape was widely adopted [3]. In this case, the formation of a radial mixing zone (RMZ) in the flame-to-flame collision area is driven by the fuel jet momentum redistribution as vortices on the jet sides [16]. The loss of kinetic energy in the adjacent jet interaction and the consequent confined air/fuel mixing in the RMZ limit the rate of combustion, minimizing the soot oxidation rate late in the cycle [17]. To modify the flame-to-flame phenomenon, Volvo has patented in 2013 the wave-shaped bowl [18], featuring radial protrusions in the regions where two adjacent flames usually collide. Guiding the near-wall flow, the new combustion system is capable of enhancing the late-cycle mixing, as widely investigated by Eismark et al. in [16] by means of both numerical and optical analyses. The key elements of the beneficial flow structures by adopting a wave bowl are summarized here below. Firstly, the radial bumps provide a more favorable collision angle between two adjacent jets, minimizing the formation of rich stagnation zones during the jet-to-jet interaction [16]. As a consequence, the retained kinetic energy in the side vortices accelerates the RMZ development toward the cylinder center, enhancing the air mixing onto the flame leading edge [16]. In addition, when the RMZ separates from the piston wall, its trailing edge shows a more efficient transport of oxidants resulting in a faster burnout [16]. The enhanced mixing mechanism for the wave bowl increases the heat release rate (HRR) in the mixing-controlled combustion, as outlined by Zhang et al. in [19]. In this work, the wave bowl has highlighted lower combustion duration with respect to a conventional bowl, leading to up to 1% thermal efficiency increment with respect to the conventional combustion system under most of the operating conditions of the European Stationary Cycle (ESC). The impact of the wave bowl is even more evident on the late-cycle soot oxidation as shown in [16], in which single-cylinder engine (SCE) tests over different partial-load operating conditions have highlighted an improved soot-NOx trade-off with 50-85% of soot reduction for the wave bowl. Moreover, if the EGR rate is increased to limit the NOx emissions, the improved mixing mechanism for the wave bowl in combination with an oxygenated fuel can give a further reduction in net soot emissions, as Eismark et al. have assessed in [20]. More recently, Belgiorno et al. have proposed an innovative diesel combustion system developed by means of steel-based additive manufacturing techniques. In particular, the combustion system was based on a highly re-entrant sharp-stepped bowl profile featuring inner radial lips. The experimental activity on the SCE test rig showed the high potential of the proposed combustion system in reducing soot emission (−25/−50%) at constant NOx level without any detrimental effect on engine efficiency [21].

Starting from the well-established benefits of the two selected piston bowl geometries, two combustion system proposals were designed: one based on the stepped-lip bowl, the other with a number of radial bumps equal to the number of the injector nozzle holes, in the outer bowl rim. The potentials of the proposed designs were investigated by means of

TABLE 1 Test engine main features.

Cylinders #	4
Displacement	1.6 L
Bore × Stroke	79.7 mm × 80.1 mm
Compression ratio	16:1
Turbocharger	Single-stage with variable geometry turbine (VGT)
Fuel injection system	Common rail max. rail pressure 2000 bar
Maximum power	100 kW at 4000 rpm
Maximum torque	320 Nm at 2000 rpm

three-dimensional Computational Fluid Dynamics (3D-CFD) simulations both in terms of turbulent flow structures and combustion development. Thanks to its predictive capability, 3D-CFD simulation has crucial importance in the development phase of the new combustion system since it provides a virtual test rig in which the potential of new engine designs can be evaluated avoiding time- and cost-consuming experimental campaigns. In this article, the simulation methodology is based on an integrated and automated 1D-/3D-CFD coupling, already validated in [22]. On one hand, the 1D-CFD models [23, 24, 25] provide the time-varying boundary conditions and a reliable injection rate profile; on the other hand, the 3D-CFD model is used to perform the in-cylinder simulations.

In the first part of the study, the in-cylinder flow structures' characterization and the mixing process for each proposed combustion system were investigated under nonreacting conditions. With this aim, the complete engine cylinder geometry was simulated considering rated power operating conditions. The swirl flow and the turbulent structures induced by the fuel injection momentum were analyzed to evaluate and quantify the piston bowls' impact on fuel mixing. Moreover, to investigate the combustion evolution, a sector mesh of the cylinder geometry was built and analyzed both at full-load and partial-load engine operating conditions. In the latter, an EGR rate sweep was performed and the combustion systems sensitivity was highlighted in terms of fuel consumption and pollutant emissions. Finally, thanks to the adoption of the detailed soot Particulate Mimic model [26, 27, 28], the soot evolution was investigated, providing a deeper understanding of the piston bowl's impact on soot formation and oxidation rates.

2. Case Study

2.1. Test Engine

The engine under investigation is a 1.6 liters diesel engine for light-duty vehicle applications, whose main characteristics are listed in Table 1. It is a four-cylinder turbocharged engine, featuring a common rail injection system and a high-pressure EGR loop. The test engine features a re-entrant piston bowl, as highlighted in Figure 1(left), and it is equipped with an eight holes solenoid injector.

FIGURE 1 Piston bowl geometries under investigation. Left: re-entrant; middle: stepped lip; right: radial bumps.

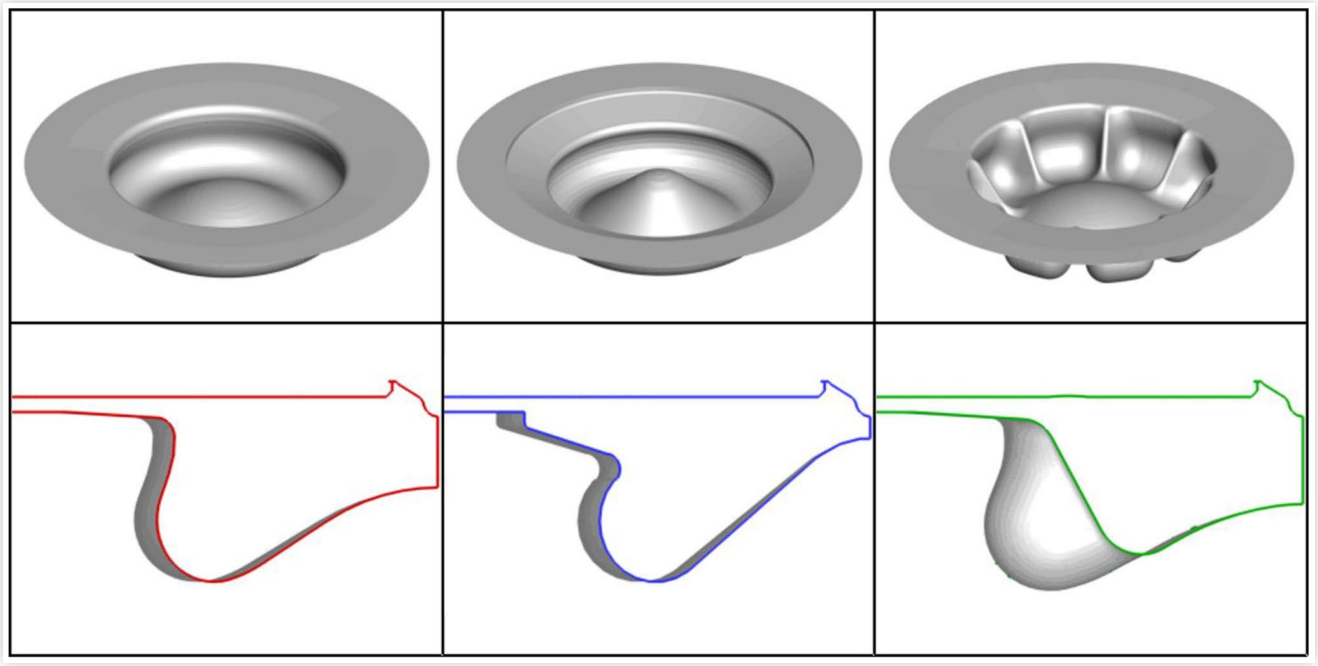

TABLE 2 Selected engine working points.

Speed [rpm]	BMEP [bar]
1500	5.0
4000	18.5

The numerical simulations were performed for two different engine working points, one at partial load, representative of the most relevant engine operating conditions during a type approval driving cycle, and one at rated power. The selected engine working points are listed in Table 2. An extensive validation of the proposed 3D-CFD model considering the baseline re-entrant bowl geometry was already presented in [22], showing a more than satisfactory accuracy in reproducing the combustion process, capturing the emission-level trend as well.

Once the predictive capabilities of the simulation setup were assessed, the stepped-lip and the radial-bumps bowl proposals were defined. The stepped-lip bowl was designed following the geometrical features in [5] while the radial-bumps bowl was designed on the basis of the re-entrant bowl, adding a number of radial bumps equal to the injector nozzle holes in the outer bowl rim, as shown in [18]. Both the proposed combustion systems feature the same bore, compression ratio, and squish height of the re-entrant bowl. Moreover, no further calibration activity was performed concerning spray targeting. Figure 1 shows the piston bowl geometries under investigation.

2.2. Simulation Setup

A previously developed and validated 1D-/3D-CFD codes coupling methodology was adopted [22]. The automated methodology is briefly presented here below: the 1D-CFD engine model, built in the commercially available software GT-SUITE and validated in [23], was used to properly initialize the first step of the multidimensional simulation, providing time-dependent boundary conditions in terms of thermodynamic conditions and species concentration. The first 3D-CFD simulation step, named "cold flow" and carried out in CONVERGE CFD, was performed to capture the local evolution in terms of pressure, temperature, and charge motion during the gas exchange process. Then starting from Intake Valve Closure (IVC), the compression stroke and the combustion process were simulated considering a single sector of the cylinder, centered along a single spray axis. The injection rate was provided thanks to a previously developed 1D-CFD injector model [24, 25], requiring as inputs only the Energizing Time, Dwell Time, and rail pressure. Finally, the results from the 3D-CFD combustion simulation were post processed by means of GT-SUITE, guaranteeing the same solution methodology as the initial 1D-CFD engine model. As far as the 3D-CFD simulation is concerned, the base grid size was selected equal to 0.50 mm, for all directions. In addition, the first-level Fixed Embedding covering the injector spray cone angle and first-level permanent Adaptive Mesh Refinement (AMR), based on velocity and temperature subgrid criterion, were set [29], thereby the resulting minimum grid size was equal to 0.25 mm. Regarding the turbulence model, the Reynolds-averaged Navier-Stokes (RANS)-based Re-Normalization Group (RNG) k-ε model [30] was adopted, while the heat transfer was simulated through the O'Rourke and Amsden model [31]. The abovementioned general settings are summarized in Table 3.

TABLE 3 General settings for the 3D-CFD simulation setup.

Base grid	0.50 mm
Minimum grid	0.25 mm
Turbulence model	RNG k-ε model
Heat transfer model	O'Rourke and Amsden

Concerning the spray model, the "blob" injection method was used [32], while the breakup of the droplets was calculated through a calibrated Kelvin-Helmholtz and Rayleigh-Taylor (KH-RT) model [32]. The submodels adopted for the spray simulation are listed in Table 4.

Considering the combustion model, the SAGE-detailed chemical kinetics solver was adopted implementing the Skeletal Zeuch mechanism, which includes the Polycyclic Aromatic Hydrocarbons (PAH) soot precursor chemistry [37], that enables the Particulate Mimic (PM) soot model for in-cylinder soot mass prediction [26, 27, 28]. Different approaches could be found in the literature for evaluating soot emissions in RANS simulation: Dempsey et al. in [38] proposed the Hiroyasu two-step soot model coupled with a semi-detailed n-heptane chemistry as a design tool for diesel engine combustion systems. However, the model tended to overpredict soot emissions, especially for radial bumps bowl. In fact, in the region of plume-to-plume interaction, the soot model predicted high soot concentrations. Table 5 summarizes the

TABLE 4 Spray submodels.

Discharge coefficient model	Cv correlation [29]
Breakup model	Calibrated KH-RT
Turbulent dispersion	O'Rourke model [33]
Collision model	No-time-counter (NTC) collision [34]
Drop drag model	Dynamic drop drag [35]
Evaporation model	Frossling model [33]
Wall film model	O'Rourke [36]

TABLE 5 Fuel surrogate, reaction mechanism, and emissions models.

Fuel species	N-heptane
Species	121
Reactions	593
PAH	(A3R5-)
Soot model	Particulate mimic
NOx	Embedded in the reaction mechanism

key elements concerning the fuel surrogate, reaction mechanism, and emissions models for the combustion simulation.

3. Numerical Analysis

3.1. Flow Structures and Air/Fuel Mixing

The combustion system effects on the in-cylinder flow field and the mixing process were investigated through CFD nonreacting simulations considering the complete cylinder geometry. The analysis was carried out considering the rated power engine operating condition since the more intense in-cylinder velocity magnitude promotes the formation of turbulent structures. The evolution of both swirl ratio (SR) and turbulent kinetic energy (TKE) for each analyzed combustion system is shown in Figure 2.

As depicted in Figure 2(top), small differences in SR evolution can be highlighted during the compression stroke up to the Start of Injection (SOI) of the pilot event: the radial-bumps bowl shows the lowest SR value due to its geometric characteristics that break the swirling motion. Going close to the Top Dead Center (TDC), it is well known that the swirl-squish interaction is the main factor in the swirl amplification [39]. In fact, the different swirl-squish interaction intensity is the main reason behind the lower swirl amplification of the stepped-lip geometry with respect to the re-entrant. As highlighted in Figure 1, the stepped lip features a lower squish area coupled with a divergent tapered lip that reduces the squish flow intensity, as reported in [40]. At TDC, the radial-bumps bowl highlights the lowest swirl amplification although it features the same squish area of the re-entrant bowl. This swirl reduction, on one side, is mainly due to the radial bumps that break the rotational swirling flow, and on the other side, it is enhanced by the high spray momentum transfer from the main injection event, causing a swirl collapse during the expansion stroke. However, by looking at Figure 2(bottom), the interaction between the swirl vortex and radial bumps distributed over the bowl rim on one side reduces the SR, but, on the other side, leads to the highest turbulence intensity during the compression stroke and the main injection event as well. Indeed, even if the turbulent structures close to TDC are mainly created by the injection event, different absolute TKE values can be observed in Figure 2(bottom), comparing the evaluated bowl designs. More specifically, the stepped-lip bowl highlights lower TKE than the re-entrant bowl, since the lower squish area provides a reduced squish flow, which is responsible for the turbulent enhancement on the bowl lip [39]. Moreover, with the re-entrant bowl, the flow separation at the bowl lip [41] and the reverse squish flow [42] can contribute to further turbulent generation.

FIGURE 2 SR (top) and TKE (bottom) evolutions for the analyzed combustion systems. Engine operating condition: 4000 RPM × 18.5 bar BMEP.

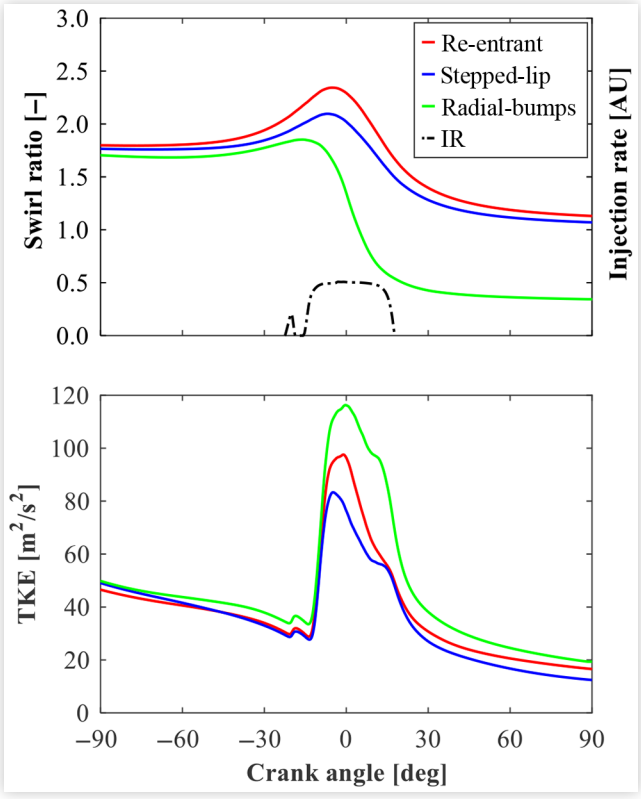

The geometrical effects on the in-cylinder flow motion and the mixing process were further investigated by analyzing the velocity and the equivalence ratio distributions. Three different planes were selected to show the numerical results, as outlined in Figure 3, in which the stoichiometric iso-surface is depicted in red clouds. Plane A is a vertical plane centered on a spray axis placed between the intake and exhaust valves in order to avoid both the valve pockets and glowplug interactions on the flow motion and in the spray evolution, respectively, while two additional planes are defined cutting two adjacent sprays placed in the exhaust side: the horizontal Plane B and Plane C, coincident with the spray axes.

To evaluate the in-cylinder flow motion, the velocity vectors on the selected planes A and B are shown in Figures 4 and 5, considering the cylinder conditions before the injection event (at −23 crank angle degrees [CAD] after TDC [aTDC]) and after the TDC when injection is occurring (at +5 CAD aTDC), respectively. Specifically, the analysis shows the velocity vectors tangential component contained in the selected cutting planes, called projected velocity, with uniform size and colored according to the projected velocity magnitude.

As already stated, Figure 4(a) clearly shows how the squish flow during the late phase of the compression stroke is affected by the piston bowl geometry: before the SOI event, the higher squish area for both the re-entrant and radial-bumps bowls leads to a more intense squish flow with respect to stepped-lip design in which the squish vortex center is

FIGURE 3 Planes selected to represent the numerical results and stoichiometric iso-surface at TDC.

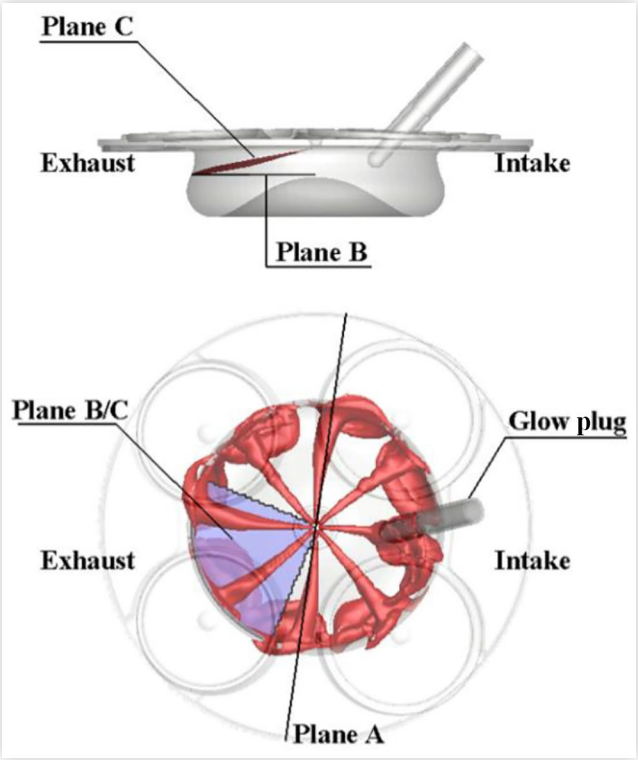

shifted on the step rim. As far as swirl motion is concerned, the flow structure is still retained for both the re-entrant and stepped-lip bowls, as shown in Figure 4(b). On the contrary, the radial-bumps design strongly affects the swirl flow: the flow separation occurred on the radial bumps enhances the turbulent generation creating a kind of "stagnation zone" for the gas within two adjacent radial bumps.

The differences in terms of flow structures are more evident during the injection event at +5 CAD aTDC, as shown in Figure 5. Velocity vectors on Plane A (Figure 5(a)) show that the toroidal vortex caused by the spray/bowl impingement and piston motion is the main flow structure in the re-entrant bowl, with a negligible fraction of the injected fuel that propagates toward the squish area. On the contrary, in the stepped-lip bowl, the fuel jet is split creating two toroidal vortices, one inward within the bowl and the other upward above the tapered step, as shown by the two black arrows. Focusing on the radial-bumps design, although it has the same bowl curvature as the re-entrant one, it shows a more pronounced toroidal vortex due to the reduced interaction between the jet and the swirl flow caused by the previously highlighted stagnation zone. High differences can be highlighted evaluating the flow velocity on Plane B in Figure 5(b). The flow structure is still swirl supported for both the re-entrant and stepped-lip bowls. Conversely, the radial-bumps design has a significant impact on the swirl flow, breaking its organized structure. In addition, due to the swirl flow, the fuel spray does not impinge on the wall in the middle between two adjacent bumps but on a higher curvature region close to the radial bumps. Thus the jet momentum is directed to the consecutive sector, and moving downstream of the bumps' tip, it drives the formation of the highly turbulent recirculating zone, as highlighted by the black arrow in Figure 5(b)(right).

The piston bowl effects on the mixture formation were investigated during the injection event on the cutting planes A/C of Figure 3, evaluating the equivalence ratio contour plots during the main injection event (+5 CAD aTDC) for the three evaluated combustion systems, as shown in Figure 6. Starting from the re-entrant bowl, Figure 6(a) depicts how the fuel jet is mainly redirected downward within the bowl, while only a reduced fuel fraction gradually propagates into the squish region, thanks to the piston motion (reverse squish). On the other hand, the fuel jet is more evenly distributed above the step and within the bowl, thanks to the stepped-lip split (Figure 6(a), middle), providing a better air utilization in the squish region and enhancing the global air/fuel mixing rate, as also confirmed by [43]. Radial-bumps bowl enhances the fuel propagation toward the piston dome, thanks to the more pronounced toroidal vortex highlighted in Figure 5. Considering the spray axes plane shown in Figure 6(b), firstly, it is worthwhile to note that the interaction between the exhaust valves and the fuel sprays results in different jet surface fluctuations. Then, evaluating the mixture formation, the re-entrant and stepped-lip bowls show a tangential fuel jet propagation on the piston surface, further enhanced by the swirl flow. As far as the jet-to-jet interaction is concerned, the re-entrant bowl shows a reduced formation of an RMZ, while, plumes interaction is not yet occurred for the stepped-lip bowl, thanks to the spray split and, consequently, to the higher upward jet velocity above the step. In addition, radial-bumps' design minimizes the jet-to-jet interaction, and the fuel is redirected by the bump into the adjacent sector, where available oxygen is present. Hence, this recirculating flow structure promotes the air/fuel mixing onto the jet front.

The equivalence ratio distribution was further investigated during the late phase of the injection event at +15 CAD aTDC, as outlined in Figure 7, in which it can be noted that the spray-wall impingement plays the main role in the flow pattern definition and, consequently, in the air/fuel mixing rate. This happens especially considering the stepped-lip bowl where the spray-wall impingement occurs above the step surface and the fuel jet mainly propagates toward the cylinder head causing poor air utilization, as highlighted in Figure 7(a). On the spray axes plane in Figure 7(b), the jet-to-jet interaction in the radial-bumps bowl continues to evolve differently from the re-entrant combustion system, indeed the recirculating flow on the bumps remains the main flow structure, with a more evident jet-to-jet interaction close to the bump rim, thus creating a more pronounced RMZ.

To further understand the piston bowl geometry effects on the mixing process, a mixing rate index was defined based on the equivalence ratio distribution within the combustion chamber. During the injection event, at each crank angle, the total cylinder mass was binned by equivalence ratio into

FIGURE 4 Velocity vectors at –23 CAD aTDC colored according to the magnitude of the projected velocity on the selected Plane A (a) and Plane B (b). Left: re-entrant; middle: stepped lip; right: radial bumps. Engine operating condition: 4000 RPM × 18.5 bar BMEP.

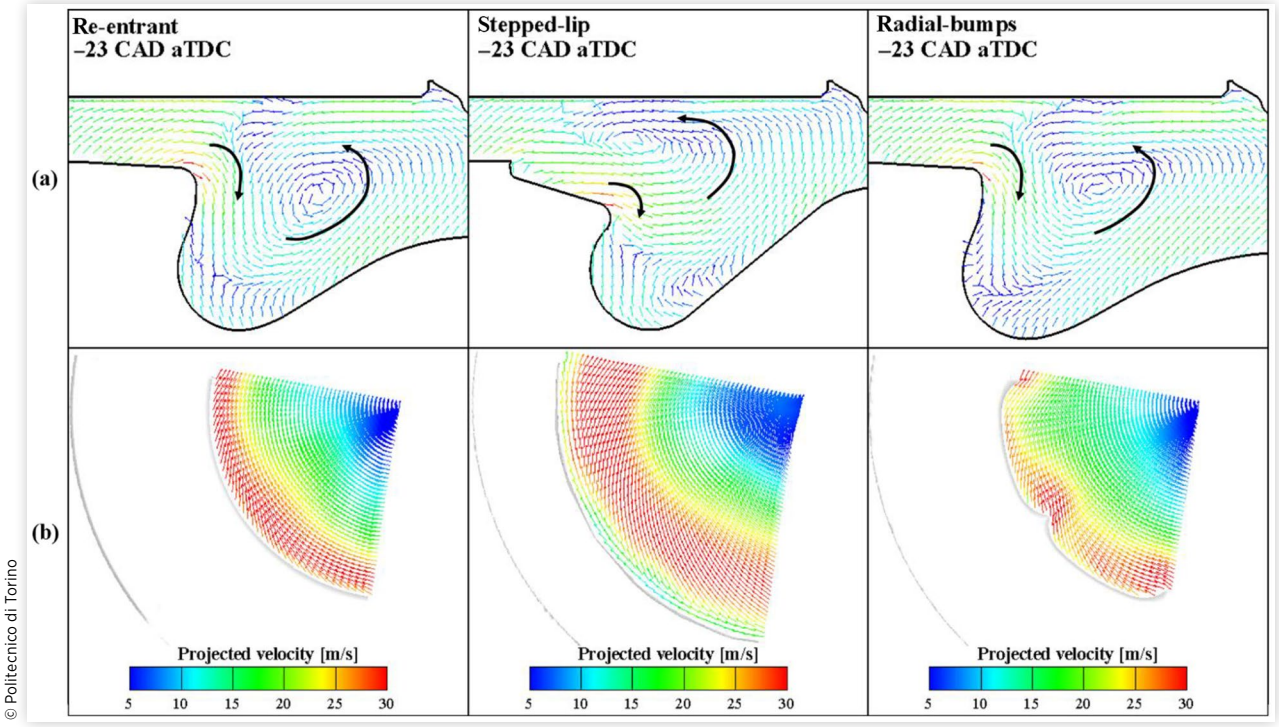

FIGURE 5 Velocity vectors at +5 CAD aTDC colored according to the magnitude of the projected velocity on the selected Plane A (a) and Plane B (b). Left: re-entrant; middle: stepped lip; right: radial bumps. Engine operating condition: 4000 RPM × 18.5 bar BMEP.

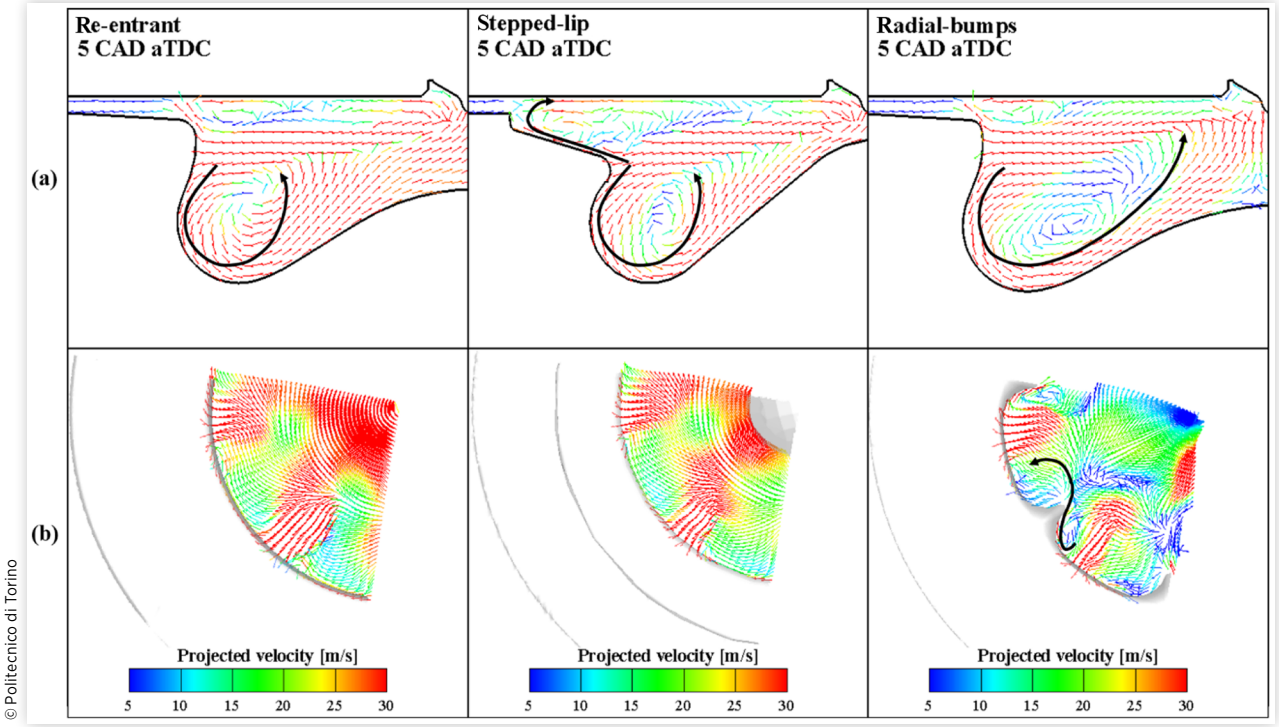

FIGURE 6 Equivalence ratio contour plot at +5 CAD aTDC on the selected Plane A (a) and Plane C (b) of Figure 3. Left: re-entrant; middle: stepped lip; right: radial bumps. Engine operating condition: 4000 RPM × 18.5 bar BMEP.

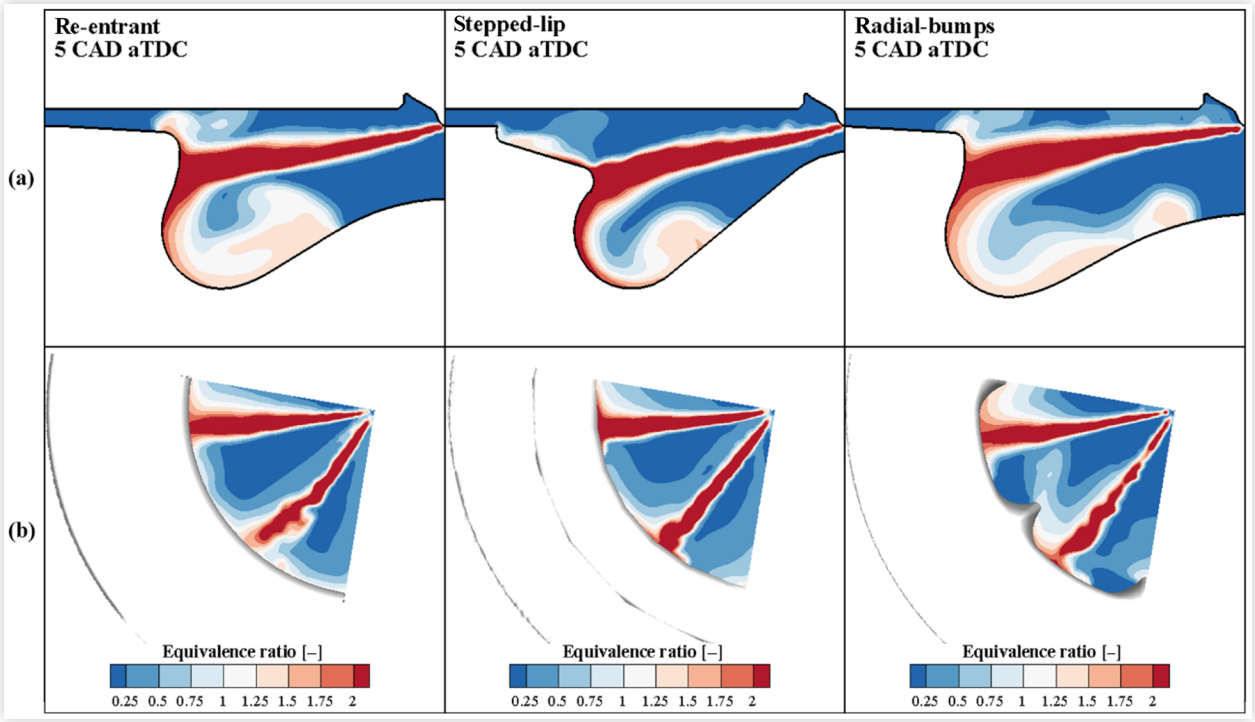

FIGURE 7 Equivalence ratio contour plot at +15 CAD aTDC on the selected Plane A (a) and Plane C (b) of Figure 3. Left: re-entrant; middle: stepped lip; right: radial bumps. Engine operating condition: 4000 RPM × 18.5 bar BMEP.

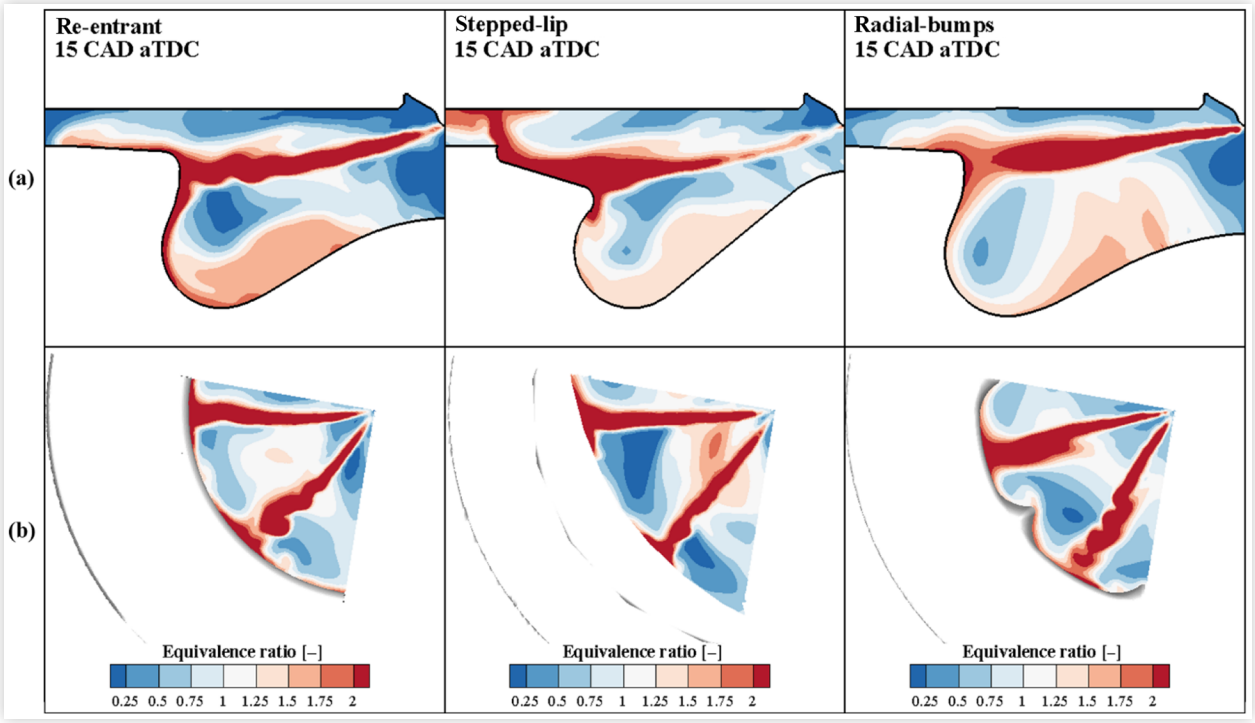

FIGURE 8 Cylinder mass fraction evolution for each equivalence ratio bin (top) and injection rate profile (bottom). Left: re-entrant; middle: stepped lip; right: radial bumps. Engine operating condition: 4000 RPM × 18.5 bar BMEP.

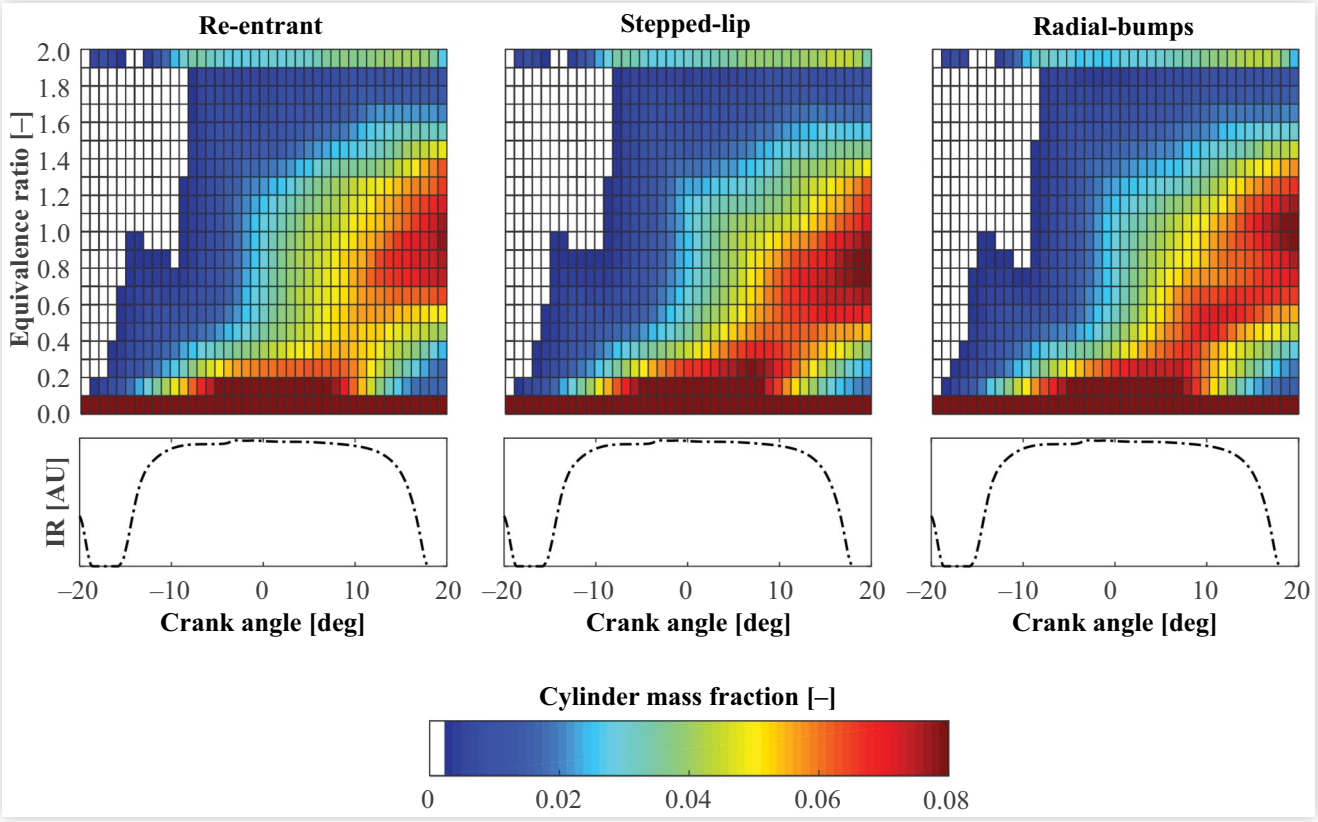

twenty intervals, starting from 0 to 0.1 bin that corresponds to pure ambient gas and ending at 1.9-2 bin that represents the injected fuel mass. Then the mass related to each bin was divided by the total cylinder mass, obtaining the cylinder mass fraction related to the corresponding bin. This latter was plotted on a bar chart, and a contour plot was defined collecting all the bar charts for each crank angle, as depicted in Figure 8. In this way, the equivalence ratio bins within the range 0.1-1 provide an index of the air/fuel mixing rate, since the higher is the cylinder mass fraction in this range the better is the air utilization. In Figure 8, during the first part of the main injection, before the TDC, no significant differences can be observed among the evaluated combustion systems, since the air/fuel mixing is mainly supported by the free propagation of the fuel jets. Approaching the TDC, the spray-wall interaction plays a crucial role in the mixing process [44] and the piston bowl effects on the equivalence ratio distribution become more evident. More specifically, from 0 to +10 CAD aTDC, both the stepped-lip and the radial-bumps bowls enhance the mixing rate with a higher cylinder mass fraction within 0.1-1 equivalence ratio bin with respect to the one obtained considering the re-entrant bowl. As already highlighted in the text, this air utilization improvement is due to the creation of two split toroidal vortices for the stepped-lip bowl, while it is linked to the fuel jet recirculation across the bumps for the radial-bumps design, as highlighted in Figure 6. During the late phase of the main injection event, from +5 CAD aTDC, the stepped-lip bowl shows a reduced mixing rate with respect to the radial bumps. In fact, the cylinder mass fraction with the stepped-lip bowl is distributed in a narrower equivalence ratio range with a higher cylinder mass fraction within the 0.2-0.4 equivalence ratio bin. This air/fuel mixing rate reduction is mainly due to the less favorable fuel split on the step, as outlined in Figure 7. Instead, the radial-bumps bowl shows a continuous increment in the air/fuel mixing, as highlighted by the spreading of cylinder mass fraction toward the stoichiometric range. This result becomes even more evident moving at the end of injection (EOI) of the main event, where, differently from the stepped-lip bowl, the faster air/fuel mixing for the radial-bumps bowl moves the peak of cylinder mass fraction toward the stoichiometric equivalence ratio.

3.2. Combustion Analysis

Full-Load Engine Operating Condition at 4000 RPM Once the impact of the different combustion systems on the air/fuel mixing process was evaluated, the combustion analysis was carried out through CFD simulations, following

FIGURE 9 Top: HRR and injection rate profile; bottom: HR. Engine operating condition (baseline): 4000 RPM × 18.5 bar BMEP.

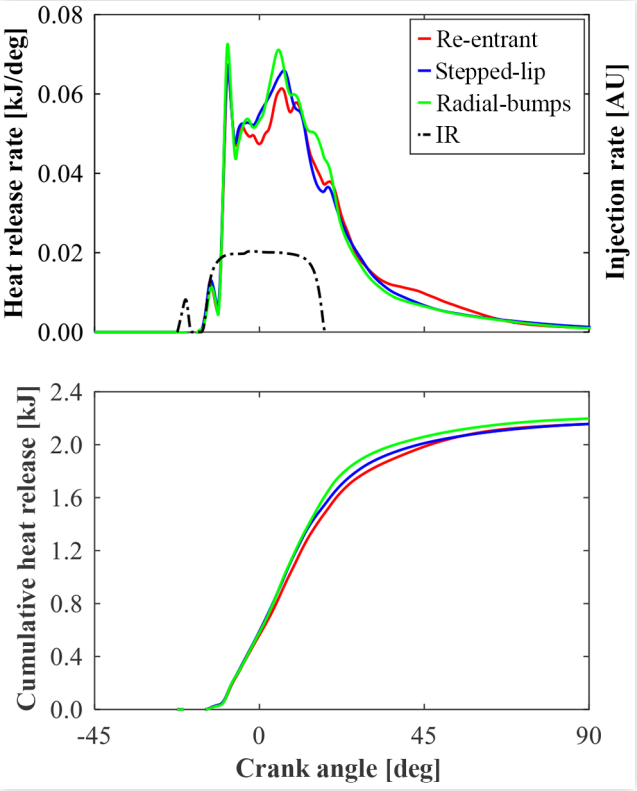

the methodology already presented in the Simulation Setup section. The analysis was performed keeping constant the injection strategy in terms of fuel mass, timing, and rail pressure in order to evaluate the brake power differences due to the combustion system. Figure 9 shows the simulations' results in terms of HRR and the cumulative heat release (HR) for the evaluated bowl designs.

Looking at the HRR (Figure 9, top), the premixed combustion phase is not highly affected by the piston bowl geometries, but going toward TDC, some differences among the bowls could be highlighted: more specifically, the re-entrant bowl shows a lower HRR with respect to stepped-lip and radial-bumps designs. In this phase, as noted by [16], the combustion development is strongly affected by the flame-to-wall and flame-to-flame events, which reduce the mixing rate onto the flame front. And as outlined in Figure 6 in nonreacting conditions, the re-entrant bowl shows the strongest jet-to-jet interaction, becoming even more evident during the combustion process due to the higher overall turbulence. From 0 to +5 CAD aTDC, the so-called mixing-controlled combustion phase starts, in which the consumption rate of the fuel is controlled by its rate of injection and its mixing with air. In this interval, the combustion results confirm the mixing analysis: both the stepped-lip and the radial-bumps bowl show a more intense HRR with respect to re-entrant design, thanks to the faster air/fuel mixing rate (see Figure 8). From +5 CAD aTDC to EOI, the HRR and the cumulative HR referred to the stepped-lip bowl drop below the radial-bumps results. In fact, as outlined in nonreacting conditions analysis, Figure 8 shows a lower mixing rate for the stepped-lip bowl due to a high fuel concentration above the step, thus reducing the air utilization within the bowl. This result is also confirmed by [45], where Kurtz et al. show that the unbalanced fuel split in a stepped-lip bowl is detrimental for the combustion efficiency, especially at high-load and high-speed conditions. On the contrary, the radial-bumps bowl shows the highest HRR in the mixing-controlled phase due to the more intense air/fuel mixing rate. After the EOI of the main event, the re-entrant HR rises close to the stepped-lip bowl, reaching a similar 10-90 combustion duration, thanks to the higher SR (see Figure 2) that efficiently mixes the residual fuel fraction. In conclusion, in keeping constant the fuel-injected quantity, the faster release of energy highlighted for the radial-bumps bowl results in a 3.3% brake power increment with respect to the re-entrant bowl while negligible difference can be observed in comparing re-entrant and stepped-lip bowls, as shown in Table 6.

TABLE 6 Brake power percentage increment with respect to the re-entrant combustion system. Engine operating condition (baseline): 4000 RPM × 18.5 bar BMEP.

	Delta brake power [%]
Stepped lip	+0.3
Radial bumps	+3.3

Partial-Load Engine Operating Condition at 1500 RPM × 5.0 bar BMEP At partial load (1500 RPM × 5.0 bar BMEP), an assessment over different EGR rates was carried out in order to identify the combustion systems' sensitivity in terms of engine-out emissions and fuel consumption. EGR rate was varied by changing the gas species fraction, thus keeping constant the volumetric efficiency and evaluating only the different dilution and thermal effects. The injection strategy was maintained unchanged except for the main event energizing time that was controlled to keep the engine load equal to the one obtained, considering baseline configuration (i.e., re-entrant bowl under the nominal EGR rate).

Figure 10 shows the typical trade-off curves for an EGR sweep: Brake-Specific Soot (BSSoot) versus Brake-Specific NOx (BSNOx) is on the left, while Brake-Specific Fuel Consumption (BSFC) versus BSNOx is on the right. The trade-offs were normalized with respect to baseline engine configuration results. It is worth to note that both the stepped-lip and radial-bumps bowls show an improved BSSoot-BSNOx trade-off with respect to the re-entrant design, and the radial-bumps bowl has not reached the typical "knee" in the trade-off, therefore suggesting a further EGR rate increase. Moreover, at baseline BSNOx, the stepped-lip and the radial-bumps bowls show, respectively, a 40% and 50% BSSoot reduction than the re-entrant bowl. As far as the BSFC-BSNOx trade-off is concerned, no significant improvement can be observed for the stepped-lip bowl, while the radial-bumps bowl shows a noticeable BSFC reduction, resulting in a 5% lower BSFC at

FIGURE 10 EGR sweep: normalized trade-offs with respect to baseline engine configuration. Left: BSSoot-BSNOx trade-off; right: BSFC-BSNOx trade-off. Engine operating condition: 1500 RPM × 5.0 bar BMEP.

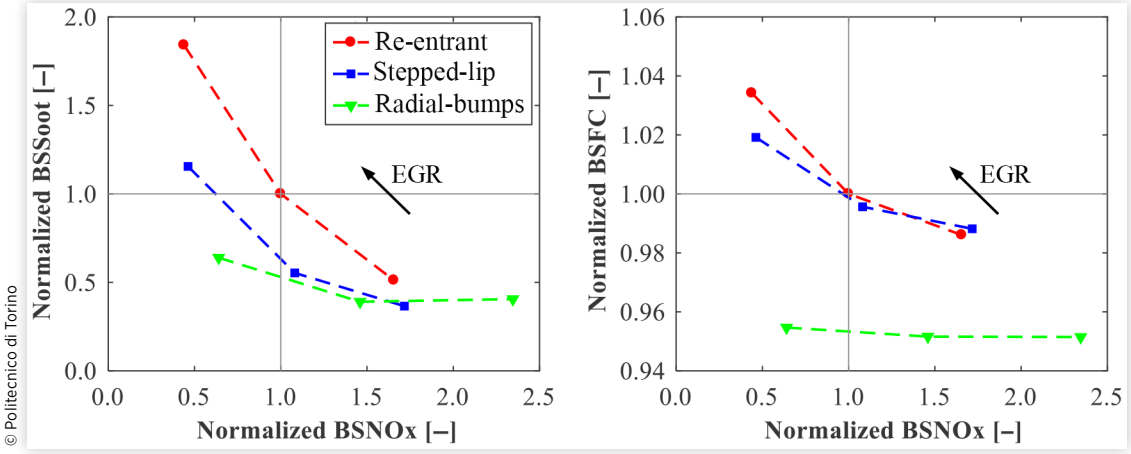

baseline BSNOx, highlighting again the unusual but desirable flatness in trade-off over the EGR sweep. To understand the reason behind the impressive BSFC reduction achieved with the radial-bumps design, the HRR for each combustion system at each simulated EGR level is shown in Figure 11. The beneficial flow motion induced by the radial bumps (highlighted in Figure 5 for rated power engine operating condition) enhances the air/fuel mixing after the main EOI (+10 CAD aTDC). Moreover, due to the swirl collapse (see Figure 2), the after-injection penetration is not affected by the organized rotational motion, thus burning within the air-rich zone close to the radial bump, further enhancing the HRR. This behavior is not affected by the EGR rate, confirming that the main driver is the improved mixing process induced by the combination of radial bumps and swirl motion. Regarding the stepped-lip bowl, an HRR enhancement with respect to the re-entrant bowl can be observed only after the EOI of the last injection event. This effect is mainly linked to the burnout of the small quantity of the after injection above the step, improving the air utilization in the squish region. However, its impact on the overall thermal efficiency is negligible, as shown in Figure 10(right).

To further understand the effect of the different combustion systems on soot formation and oxidation process, the soot evolution along the engine cycle under nominal EGR rate was investigated. The results from the detailed PM model in terms of soot mass and net soot formation rate are shown in Figure 12. After the EOI of the main event, soot mass from radial-bumps bowl drops under the values obtained with re-entrant and stepped-lip bowls. In fact, minimizing the flame-to-flame interaction and enhancing the air/fuel mixing onto the flame front, resulting in a significant reduction of net soot formation rate (as shown in Figure 12, bottom). During the after-injection burnout, the soot mass and its net formation rate from the stepped lip are higher with respect to the re-entrant bowl. However, going ahead in the engine cycle, when the burn-out of the residual rich pockets has crucial importance on the soot oxidation rate [17], the stepped-lip

FIGURE 11 HRR for the EGR sweep and partial-load injection rate profile. Engine operating condition: 1500 RPM × 5.0 bar BMEP.

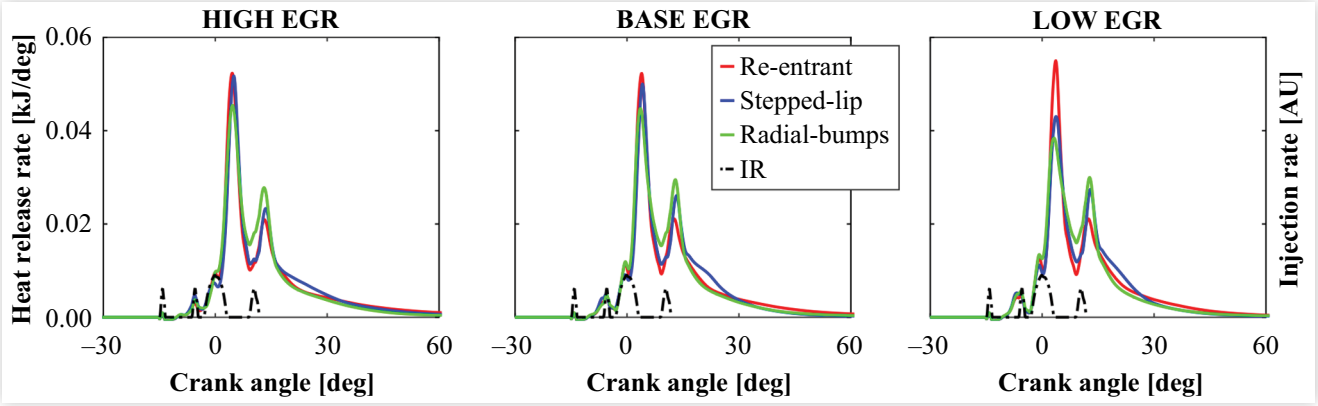

FIGURE 12 Soot PM model results for the nominal EGR rate. Top: In-cylinder soot mass; bottom: Net formation rate of in-cylinder soot mass. Engine operating condition: 1500 RPM × 5.0 bar BMEP.

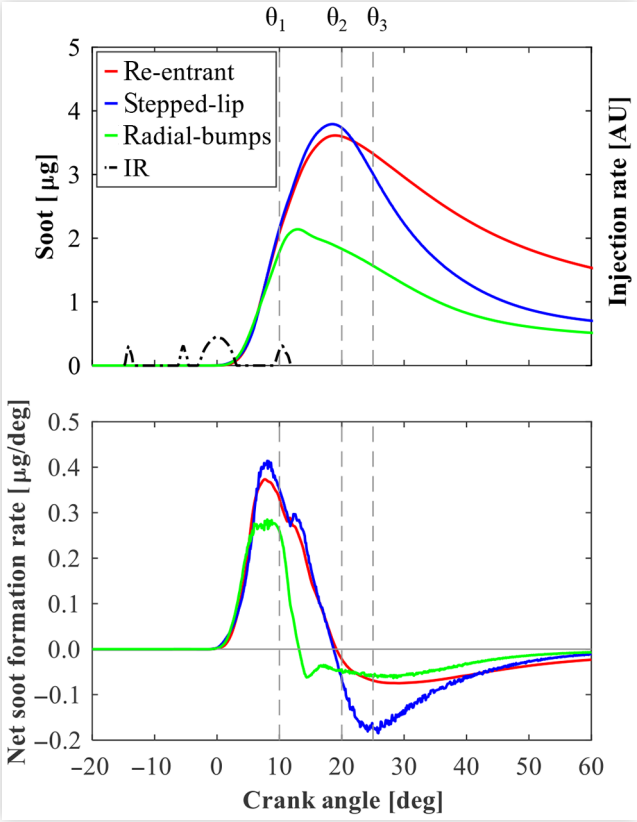

bowl shows the highest soot oxidation rate, reaching a comparable engine-out soot level than with the radial bumps.

As highlighted in Figure 12, both the innovative solutions have provided a remarkable reduction in terms of engine-out soot emissions, although both the mixing and the combustion processes were found to be quite different. Therefore, a deeper investigation was carried on the soot emission, analyzing its in-cylinder evolution history. More in detail: the mass of the computational domain was divided into classes (or bins) accordingly to the soot mass density of each cell, considering, as a reference, the maximum soot density obtained with the re-entrant bowl. The in-cylinder mass characterized by a soot density between 20% and 40% of the maximum value (Bin #1) was considered representative of a low-soot density class, while the mass within 60-80% of the maximum soot density value (Bin #2) was selected to depict the high-soot density class. Figure 13 shows Bin #1 (blue) and Bin #2 (red) soot density iso-surfaces at three different CADs highlighted in Figure 12.

At θ_1 = +10 CAD aTDC. Figure 13(a) shows the soot density distribution for each evaluated bowl after the main EOI. Both re-entrant and the stepped-lip bowls highlight a larger red zone into the sector periphery due to the flame-to-flame interaction previously stated. On the contrary, the radial bumps allow the minimization of this counterproductive effect enhancing the mixing rate in the sector periphery, where lower soot density can be observed. Moreover, differently from the other combustion systems, the more pronounced tumbling vortex (see Figure 5) drags the combustion, and consequently, the Bin #2 high-soot iso-surface toward the cylinder center, where the available oxygen will promote soot oxidation.

At θ_2 = +20 CAD aTDC. The effects of the after-injection burnout are highlighted in Figure 13(b). The re-entrant design partially oxides soot, mainly thanks to the temperature increment promoted by the after injection combustion. In the stepped-lip bowl, the flame jet is directed above the step where almost the total after injection combustion occurs. In addition, due to the higher bowl curvature, the flame recirculation within the bowl strongly interacts with the after-injection flame on the spray axis, increasing the Bin #2 high-soot iso-surface. Regarding the radial-bumps bowl, both the after-injection burnout and the flame propagation toward the piston dome, contribute to a more efficient oxidation process, and the Bin #2 iso-surface is totally oxidized.

At θ_3 = +25 CAD aTDC. Moving ahead in the engine cycle, all the combustion systems show the oxidation of the higher soot density mass, as outlined in Figure 13(c). More specifically, the stepped-lip bowl significantly improves the oxidation rate compared to the other designs, as also shown from the net soot formation rate in Figure 12(bottom). The soot oxidation is promoted by a side effect of the after injection above the step: in fact, on one side, there is a higher soot formation in the squish region, but on the other side, the previously injected fuel burns in the dome region where the available oxygen helps the soot oxidation, as also highlighted in [43]. Additionally, the higher bowl curvature increases the upward velocity of the flame flowing within the bowl, and the resulting turbulent structure, highlighted by the Bin #1 iso-surface wrinkling, enhances the mixing rate. Contrarily, for the re-entrant bowl, the residual soot mass oxidation is mainly driven by a well-organized toroidal flow structure, leading to a slower mixing late in the cycle, as also assessed in [15].

4. Conclusions

In this work, the effects of three different piston bowl geometries (re-entrant, stepped lip, and radial bumps) for a swirl-supported light-duty diesel engine were assessed by means of numerical simulations. The investigation was divided into two main steps: nonreacting conditions were analyzed at rated power to understand the mechanisms that drive the air/fuel mixing process. Then the combustion analysis was carried out at both rated power and partial-load engine operating points to highlight the impact of combustion systems on the

FIGURE 13 Bin #1 (blue) and Bin #2 (red) soot density iso-surfaces under the nominal EGR rate. The liquid fuel is represented by the black parcels. Left: re-entrant; middle: stepped lip; right: radial bumps. Engine operating condition: 1500 RPM × 5.0 bar BMEP.

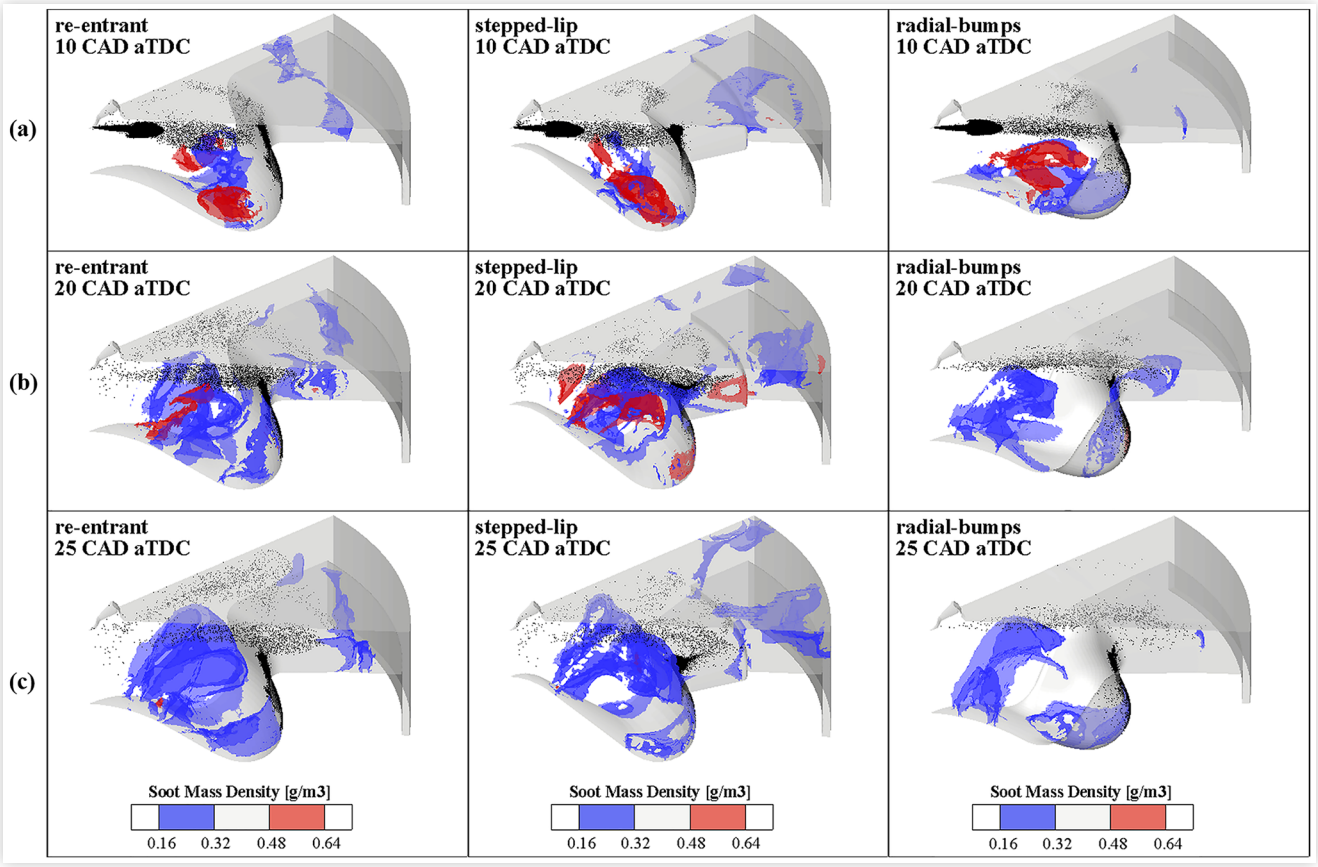

energy release and soot formation and oxidation phenomena. The main differences between stepped-lip and radial-bumps designs with respect to a conventional re-entrant bowl can be summarized as follows:

- In nonreacting conditions, both the combustion systems highlighted an improved air/fuel mixing. The stepped-lip bowl showed the formation of two toroidal vortices, upward above the step and inward into the bowl, increasing the air utilization on the squish region. However, an optimized spray targeting is the key to avoid an unbalanced fuel split above the step. Conversely, a strong interaction was observed between the radial bumps and the swirling flow, on one side leading to a jet-to-jet interaction minimization and on the other side increasing the overall turbulence. In addition, the coupling effect of radial bumps and swirling flow was found to be beneficial to promote the fuel jet recirculation downstream of the bump tip, where the available oxygen could enhance the air/fuel mixing.
- Combustion simulations at rated power have confirmed the nonreacting results, with an air/fuel mixing improvement near TDC. However, in the stepped-lip bowl, the nonoptimal spray targeting resulted in an HRR slowdown. On the contrary, the radial-bumps bowl showed the highest rate of energy release since the combustion was driven by the improved mixing, with a 3.3% brake power increment with respect to the re-entrant bowl.
- At partial-load engine operating conditions, the innovative piston bowls showed a noticeable improvement in Soot-NOx trade-off over an EGR sweep. In fact, at the baseline BSNOx, the stepped lip and the radial bumps provided a 40% and 50%, respectively, soot reduction with respect to the re-entrant bowl. As far as the BSFC-BSNOx trade-off is concerned, no significant deviation was observed for the stepped lip, while 5% BSFC reduction was achieved thanks to the radial-bumps design that highlighted the beneficial flatness in the trade-off curve over the EGR sweep.

Finally, future analysis will be aimed at the experimental assessment of the proposed innovative combustion systems by means of both optical and metal engines to validate the main outcomes under real engine operating conditions.

Contact Information

Prof. Federico Millo
Energy Department
Politecnico di Torino
c.so Duca degli Abruzzi, 24
10129 Torino - ITALY
federico.millo@polito.it

Acknowledgments

Computational resources were provided by HPC@POLITO, a project of Academic Computing within the Department of Control and Computer Engineering at the Politecnico di Torino (http://www.hpc.polito.it).

Abbreviations

AMR - Adaptive Mesh Refinement
BMEP - Brake Mean Effective Pressure
BSFC - Brake-Specific Fuel Consumption
BSNOx - Brake-Specific NOx
BSSoot - Brake-Specific Soot
CAD aTDC - Crank Angle Degrees after Top Dead Center
CFD - Computational Fluid Dynamics
CIV - Combustion Image Velocimetry
ECN - Engine Combustion Network
EGR - Exhaust Gas Recirculation
EOI - End Of Injection
ESC - European Stationary Cycle
HR - Cumulative Heat Release
HRR - Heat Release Rate
IVC - Intake Valve Closure
KH-RT - Kelvin-Helmholtz and Rayleigh-Taylor
NL - Natural Luminosity
NTC - No Time Counter
PAH - Polycyclic Aromatic Hydrocarbons
PM - Particulate Mimic
RANS - Reynolds-Averaged Navier-Stokes
RMZ - Radial Mixing Zone
RNG - Re-Normalization Group
SCE - Single-Cylinder Engine
SOI - Start Of Injection
SR - Swirl Ratio
TDC - Top Dead Center
TKE - Turbulent Kinetic Energy
VGT - Variable Geometry Turbine

References

1. ICCT, "Shifting Gears: The Effects of a Future Decline in Diesel Market Share on Tailpipe CO_2 and NOX Emissions in Europe," 2017.
2. Sanchez, F.P., Bandivadekar, A., and German, J., "Estimated Cost of emission Reduction Technologies for LDVs," *Int. Counc. Clean Transp.* (Mar.):1-136, 2012, https://theicct.org/sites/default/files/publications/ICCT_LDVcostsreport_2012.pdf.
3. Andersson, Ö. and Miles, P.C., "Diesel and Diesel LTC Combustion," *Encyclopedia of Automotive Engineering* (2014), 1-36, Wiley Online Library, https://doi.org/10.1002/9781118354179.auto120.
4. Miles, P.C., and Andersson, Ö., "A Review of Design Considerations for Light-Duty Diesel Combustion Systems," *International Journal of Engine Research* 17(1):6-15, 2016, https://doi.org/10.1177/1468087415604754.
5. Cornwell, R. and Conicella, F., "Direct Injection Diesel Engines," U.S. Patent 8770168 B2, Ricardo UK Limited, West Sussex (GB), 2014.
6. Styron, J., Baldwin, B., Fulton, B., Ives, D. et al., "Ford 2011 6.7L Power Stroke® Diesel Engine Combustion System Development," SAE Technical Paper 2011-01-0415, 2011, https://doi.org/10.4271/2011-01-0415.
7. Yoo, D., Kim, D., Jung, W., Kim, N. et al., "Optimization of Diesel Combustion System for Reducing PM to Meet Tier4-Final Emission Regulation without Diesel Particulate Filter," SAE Technical Paper 2013-01-2538, 2013, https://doi.org/10.4271/2013-01-2538.
8. Kogo, T., Hamamura, Y., Nakatani, K., Toda, T. et al., "High Efficiency Diesel Engine with Low Heat Loss Combustion Concept - Toyota's Inline 4-Cylinder 2.8-Liter ESTEC 1GD-FTV Engine," SAE Technical Paper 2016-01-0658, 2016, https://doi.org/10.4271/2016-01-0658.
9. Lückert, P., Arndt, S., Duvinage, F., Kemmner, M. et al., "The New Mercedes-Benz 4-Cylinder Diesel Engine OM654—The Innovative Base Engine of the New Diesel Generation," in *24th Aachen Colloquium Automobile and Engine Technology*, Aachen, Germany, 2015, 867-892.
10. Millo, F., Piano, A., Peiretti Paradisi, B., Boccardo, G. et al., "The Effect of Post Injection Coupled with Extremely High Injection Pressure on Combustion Process and Emission Formation in an Off-Road Diesel Engine: A Numerical and Experimental Investigation," SAE Technical Paper 2019-24-0092, 2019, https://doi.org/10.4271/2019-24-0092.
11. Busch, S., Zha, K., Perini, F., Reitz, R. et al., "Bowl Geometry Effects on Turbulent Flow Structure in a Direct Injection Diesel Engine," SAE Technical Paper 2018-01-1794, 2018, https://doi.org/10.4271/2018-01-1794.
12. Busch, S., Zha, K., Kurtz, E., Warey, A. et al., "Experimental and Numerical Studies of Bowl Geometry Impacts on Thermal Efficiency in a Light-Duty Diesel Engine," SAE Technical Paper 2018-01-0228, 2018, https://doi.org/10.4271/2018-01-0228.

13. Zha, K., Busch, S., Warey, A., Peterson, R. et al., "A Study of Piston Geometry Effects on Late-Stage Combustion in a Light-Duty Optical Diesel Engine Using Combustion Image Velocimetry," *SAE Int. J. Engines* 11(6):783-804, 2018, https://doi.org/10.4271/2018-01-0230.
14. Sandia National Laboratories, "Piston Bowl Geometry Study," https://ecn.sandia.gov/engines/small-bore-diesel-engine/experimental-data/piston-bowl-geometry-study/, accessed May 2020.
15. Perini, F., Busch, S., Zha, K., Reitz, R. et al., "Piston Bowl Geometry Effects on Combustion Development in a High-Speed Light-Duty Diesel Engine," SAE Technical Paper 2019-24-0167, 2019, https://doi.org/10.4271/2019-24-0167.
16. Eismark, J., Andersson, M., Christensen, M., Karlsson, A. et al., "Role of Piston Bowl Shape to Enhance Late-Cycle Soot Oxidation in Low-Swirl Diesel Combustion," *SAE Int. J. Engines* 12(3):233-249, 2019, https://doi.org/10.4271/03-12-03-0017.
17. Eismark, J., Balthasar, M., Karlsson, A., Benham, T. et al., "Role of Late Soot Oxidation for Low Emission Combustion in a Diffusion-Controlled, High-EGR, Heavy Duty Diesel Engine," SAE Technical Paper 2009-01-2813, 2009, https://doi.org/10.4271/2009-01-2813.
18. Eismark, J. and Balthasar, M., "Device for Reducing Emissions in a Vehicle Combustion Engine," U.S. Patent 8499735B2, Volvo Lastvagnar AB, Göteborg (SE), 2013.
19. Zhang, T., Eismark, J., Munch, K., and Denbratt, I., "Effects of a Wave-Shaped Piston Bowl Geometry on the Performance of Heavy Duty Diesel Engines Fueled with Alcohols and Biodiesel Blends," *Renewable Energy* 148:512-522, 2020, https://doi.Org/10.1016/j.renene.2019.10.057.
20. Eismark, J., Christensen, M., Andersson, M., Karlsson, A. et al., "Role of Fuel Properties and Piston Shape in Influencing Soot Oxidation in Heavy-Duty Low Swirl Diesel Engine Combustion," *Fuel* 254:115568, 2019, https://doi.Org/10.1016/j.fuel.2019.05.151.
21. Belgiorno, G., Boscolo, A., Dileo, G., Numidi, F. et al., "Experimental Study of Additive-Manufacturing-Enabled Innovative Diesel Combustion Bowl Features for Achieving Ultra-Low Emissions and High Efficiency," SAE Technical Paper 2020-37-0003, 2020, https://doi.org/10.4271/2020-37-0003.
22. Millo, F., Piano, A., Peiretti Paradisi, B., Marzano, M.R. et al., "Development and Assessment of an Integrated 1D-3D CFD Codes Coupling Methodology for Diesel Engine Combustion Simulation and Optimization," *Energies* 13:1612, 2020, https://doi.org/10.3390/en13071612.
23. Piano, A., Millo, F., Boccardo, G., Rafigh, M. et al., "Assessment of the Predictive Capabilities of a Combustion Model for a Modern Common Rail Automotive Diesel Engine," SAE Technical Paper 2016-01-0547, 2016, https://doi.org/10.4271/2016-01-0547.
24. Piano, A., Millo, F., Postrioti, L., Biscontini, G. et al., "Numerical and Experimental Assessment of a Solenoid Common-Rail Injector Operation with Advanced Injection Strategies," *SAE Int. J. Engines* 9(1):565-575, 2016, https://doi.org/10.4271/2016-01-0563.
25. Piano, A., Boccardo, G., Millo, F., Cavicchi, A. et al., "Experimental and Numerical Assessment of Multi-Event Injection Strategies in a Solenoid Common-Rail Injector," *SAE Int. J. Engines* 10(4):2129-2140, 2017, https://doi.org/10.4271/2017-24-0012.
26. Frenklach, M., and Wang, H., "Detailed Modeling of Soot Particle Nucleation and Growth," *Symposium (International) on Combustion* 23(1):1559-1566, 1991, https://doi.org/10.1016/S0082-0784(06)80426-1.
27. Kazakov, A., Wang, H., and Frenklach, M., "Detailed Modeling of Soot Formation in Laminar Premixed Ethylene Flames at a Pressure of 10 Bar," *Combustion and Flame* 100(1-2):111-120, 1995, https://doi.org/10.1016/0010-2180(94)00086-8.
28. Kazakov, A., and Frenklach, M., "Dynamic Modeling of Soot Particle Coagulation and Aggregation: Implementation with the Method of Moments and Application to High-Pressure Laminar Premixed Flames," *Combustion and Flame* 114(3-4):484-501, 1998, https://doi.org/10.1016/S0010-2180(97)00322-2.
29. Richards, K.J., Senecal, P.K., and Pomraning, E., *Converge 2.3 Manual* (Madison, WI: Convergent Science Inc., 2016).
30. Orszag, S.A., Yakhot, V., Flannery, W.S., Boysan, F. et al., "Renormalization Group Modeling and Turbulence Simulations," *Near-Wall Turbulent Flows* 13:1031-1046, 1993.
31. Amsden, A.A., "KIVA-3V: A Block Structured KIVA Program for Engines with Vertical or Canted Valves," Technical Report LA-13313-MS, Los Alamos National Laboratory, 1997.
32. Reitz, R.D., and Bracco, F.V., "Mechanisms of Breakup of Round Liquid Jets," *Encyclopedia of Fluid Mechanism* 3:233-249, 1986.
33. Amsden, A.A., O'Rourke, P.J., and Butler, T.D., "KIVA-II: A Computer Program for Chemically Reactive Flows with Sprays," Technical Report LA-11560-MS, Los Alamos National Laboratory, 1989.
34. Schmidt, D.P., and Rutland, C.J., "A New Droplet Collision Algorithm," *Journal of Computational Physics* 164(1):62-80, 2000, https://doi.org/10.1006/jcph.2000.6568.
35. O'Rourke, P., and Amsden, A., "The Tab Method for Numerical Calculation of Spray Droplet Breakup," SAE Technical Paper 872089, 1987, https://doi.org/10.4271/872089.
36. O'Rourke, P., and Amsden, A., "A Spray/Wall Interaction Submodel for the KIVA-3 Wall Film Model," SAE Technical Paper 2000-01-0271, 2000, https://doi.org/10.4271/2000-01-0271.
37. Zeuch, T., Moréac, G., Ahmed, S.S., and Mauss, F., "A Comprehensive Skeletal Mechanism for the Oxidation of n-Heptane Generated by Chemistry-Guided Reduction," *Combustion and Flame* 155(4):651-674, 2008, https://doi.Org/10.1016/j.combustflame.2008.05.007.

38. Dempsey, A., Seiler, P., Svensson, K., and Qi, Y., "A Comprehensive Evaluation of Diesel Engine CFD Modeling Predictions Using a Semi-Empirical Soot Model over a Broad Range of Combustion Systems," *SAE Int. J. Engines* 11(6):1399-1420, 2018, https://doi.org/10.4271/2018-01-0242.
39. Miles, P.C., "Turbulent Flow Structure in Direct-Injection, Swirl-Supported Diesel Engines," in Arcoumanis, C. and Kamimoto, T. (eds), *Flow and Combustion in Reciprocating Engines*, Experimental Fluid Mechanics (Berlin, Heidelberg: Springer, 2008), https://doi.org/10.1007/978-3-540-68901-0_4.
40. Perini, F., Zha, K., Busch, S., Kurtz, E. et al., "Piston Geometry Effects in a Light-Duty, Swirl-Supported Diesel Engine: Flow Structure Characterization," *International Journal of Engine Research* 19(10):1079-1098, 2018, https://doi.org/10.1177/1468087417742572.
41. Celik, I., Yavuz, I., Smirnov, A., Smith, J. et al., "Prediction of In-Cylinder Turbulence for IC Engines," *Combustion Science and Technology* 153(1):339-368, 2000, https://doi.org/10.1080/00102200008947269.
42. Lin, L., Shulin, D., Jin, X., Jinxiang, W. et al., "Effects of Combustion Chamber Geometry on In-Cylinder Air Motion and Performance in DI Diesel Engine," SAE Technical Paper 2000-01-0510, 2000, https://doi.org/10.4271/2000-01-0510.
43. Dolak, J., Shi, Y., and Reitz, R., "A Computational Investigation of Stepped-Bowl Piston Geometry for a Light Duty Engine Operating at Low Load," SAE Technical Paper 2010-01-1263, 2010, https://doi.org/10.4271/2010-01-1263.
44. Pickett, L., and López, J., "Jet-Wall Interaction Effects on Diesel Combustion and Soot Formation," SAE Technical Paper 2005-01-0921, 2005, https://doi.org/10.4271/2005-01-0921.
45. Kurtz, E., and Styron, J., "An Assessment of Two Piston Bowl Concepts in a Medium-Duty Diesel Engine," *SAE Int. J. Engines* 5(2):344-352, 2012, https://doi.org/10.4271/2012-01-0423.